HHS Public Access

Author manuscript

Cell Rep. Author manuscript; available in PMC 2017 October 30.

Published in final edited form as:

Cell Rep. 2017 October 17; 21(3): 758–772. doi:10.1016/j.celrep.2017.09.067.

The conserved RNA exonuclease Rexo5 is required for 3′ end maturation of 28S rRNA, 5S rRNA, and snoRNAs

Stefanie Gerstberger[1], **Cindy Meyer**[1], **Sigi Benjamin-Hong**[2], **Joe Rodriguez**[2], **Daniel Briskin**[1], **Claudia Bognanni**[1], **Kimberly Bogardus**[1], **Hermann Steller**[2,*], and **Thomas Tuschl**[1,3,*]

[1]Howard Hughes Medical Institute, Laboratory of RNA Molecular Biology, The Rockefeller University, New York, NY 10065, USA

[2]Strang Laboratory of Apoptosis and Cancer Biology, The Rockefeller University, New York, NY 10065, USA

SUMMARY

Non-coding RNA biogenesis in higher eukaryotes has not been fully characterized. Here, we studied the Drosophila melanogaster Rexo5 (CG8368) protein, a metazoan-specific member of the DEDDh 3′-5′ single-stranded RNA exonucleases, by genetic, biochemical, and RNA sequencing approaches. Rexo5 is required for small nucleolar RNA (snoRNA) and ribosomal RNA (rRNA) biogenesis, and is essential in D. melanogaster. Loss-of-function mutants accumulate improperly 3′-end-trimmed 28S rRNA, 5S rRNA, and snoRNA precursors in vivo. Rexo5 is ubiquitously expressed at low levels in somatic metazoan cells, but extremely elevated in male and female germ cells. Loss of Rexo5 leads to increased nucleolar size, genomic instability, defective ribosome subunit export and larval death. Loss-of-germline expression compromises gonadal growth and meiotic entry during germline development.

eTOC blurb

[*]Correspondence: ttuschl@rockefeller.edu. [*]Correspondence: steller@rockefeller.edu.
[3]Lead author

AUTHORS CONTRIBUTION

S.G. designed, performed experiments, analyzed data and wrote the manuscript. C.M. performed some cell culture experiments and edited the manuscript. S.B.H. and J.R. assisted with confocal imaging and edited the manuscript. D.B. and K.B. prepared some of the hydrolysis-based small RNA-seq libraries. C.B. synthesized the RNA-FISH probes. H.S. and T.T. provided general oversight, analyzed data, and edited the manuscript.

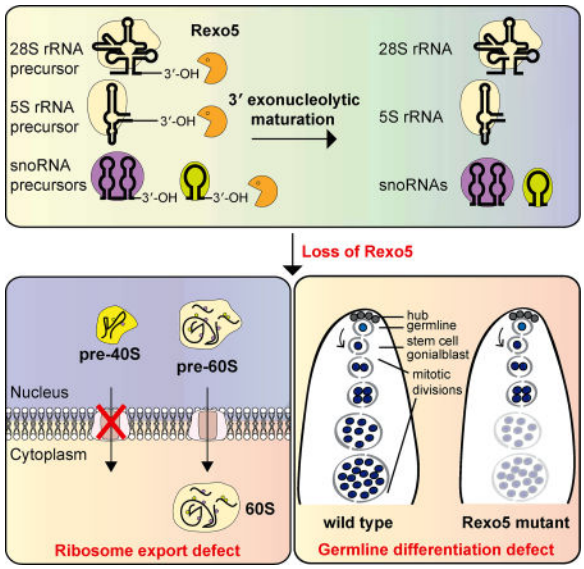

Gerstberger *et al.* adapt hydrolysis-based small-RNA-sequencing to identify RNA targets of the conserved 3'-5' RNA exonuclease Rexo5 in *Drosophila melanogaster*. Rexo5 was revealed as key factor in snoRNA, 28S and 5S rRNA 3' end maturation. Loss-of-function of Rexo5 leads to impaired ribosomal export and germline developmental defects.

Keywords

rRNA biogenesis; rRNA 3′ end maturation; rRNA processing; snoRNA biogenesis; snoRNA 3′ end maturation; snoRNA processing; RNA exonuclease; U8 snoRNA

INTRODUCTION

Ribosome biogenesis is central to protein synthesis and perhaps the most complex RNA metabolic process in eukaryotic cells, involving more than 200 ribosomal proteins and assembly factors in Saccharomyces cerevisiae and over 400 in human cells (Lafontaine, 2015; Tafforeau et al., 2013). Precursor ribosomal RNA (pre-rRNA) processing is conserved among eukaryotes, but with increasing organismal complexity additional proteins and processing pathways evolved in speciation (Henras et al., 2014).

Transcription, processing, and ribosomal subunit assembly are confined to the nucleolus. The 8–13 kb long 47S rRNA precursor transcript (37S in S. cerevisiae) contains 18S, 5.8S, and 28S rRNAs and is transcribed from multi-copy rDNA loci by RNA polymerase (Pol) I (Miller and Beatty, 1969; Mullineux and Lafontaine, 2012). The 47S pre-rRNA is co- and post-transcriptionally processed resulting in removal of the 5′ and 3′ external transcribed spacers (5′-ETS, 3′-ETS), and the internal transcribed spacer 1 and 2 (ITS1, ITS2) (Figure 1). The precursor of 5S rRNA is transcribed separately by RNA Pol III in the nucleus from a multi-copy 5S rDNA array (Ciganda and Williams, 2011). C/D and H/ACA small nucleolar RNA (snoRNA) ribonucleoprotein complexes introduce site-specific 2′-O-methylation and pseudouridylation into rRNAs, which determine rRNA folding, translational activity, and

innate nucleic-acid-sensing (Roers et al., 2016; Sharma and Lafontaine, 2015). A subset of snoRNAs, including U3 and the metazoan-specific U8, are essential for rRNA processing, guiding cleavage in the 5′-ETS, ITS1 and 3′-ETS (Watkins and Bohnsack, 2012). rRNAs and ribosomal proteins are further assembled into the two ribosomal subunits: 18S rRNA into the small 40S, and 28S, 5.8S, and 5S rRNAs into the large 60S ribosomal subunit.

3′ end formation of 5S rRNA is uncharacterized in metazoans. In S. cerevisiae the 3′ trailer of 5S pre-rRNA is exonucleolytically removed by Rex1p (RNH70/RNA82/REX1) (Piper et al., 1983; 1984). Rex1p is a nonessential gene, though deletion strains accumulate improperly 3′-end-processed 5S rRNAs (Elela et al., 1996; Kufel et al., 1999; Piper et al., 1983; van Hoof et al., 2000).

Transcription termination and 3′ end processing of the 47S pre-rRNA shows species-specific differences (Gurney, 1985; Kuhn and Grummt, 1989; Labhart and Reeder, 1986; Mullineux and Lafontaine, 2012; Tautz and Dover, 1986). In S. cerevisiae, the 37S pre-rRNA is co-transcriptionally cleaved by the double-stranded RNA (dsRNA) endonuclease Rnt1p in the 3′-ETS, 10–20 nt downstream of 28S rRNA at B0 (Figure 1) (Elela et al., 1996). The residual 3′-ETS is 3′-5′ exonucleolytically removed by Rex1p during late ribosome biogenesis (Kempers-Veenstra et al., 1986; Kressler et al., 1999). In contrast, the mammalian Rnt1p ortholog Drosha processes double-stranded microRNA precursors in the nucleus (Lee et al., 2003). Knockdown of Drosha in human cells and genetic knockouts in mice and D. melanogaster showed unaltered mature and 47S pre-rRNA levels (Chong et al., 2008; Smibert et al., 2011; Wu et al., 2000).

In D. melanogaster and vertebrates, cleavage at site 02 removes the 3′-ETS (Figure 1) (Long and Dawid, 1980; Mandal and Dawid, 1981; Mullineux and Lafontaine, 2012). Removal of the 3′-ETS was studied in Xenopus laevis, where 45S pre-rRNA is the only detectable intermediate at steady state conditions as the 47S precursor is rapidly processed at T1 (02 in mammals) (Figure 1) (Labhart and Reeder, 1987). Processing at T1 is thought to require an endonucleolytic cleavage reaction by an unknown nuclease and is dependent on U8 snoRNA (Peculis and Steitz, 1993). In U8-depleted X. laevis oocytes, mature 28S rRNA was undetectable in cytoplasmic fractions and incompletely 3′-end-trimmed 32S and 36S pre-rRNA intermediates accumulated in the nuclear fraction (Peculis and Steitz, 1993). U8 snoRNA is conserved between invertebrates and vertebrates and implicated in long-range pre-rRNA folding, facilitating 3′-ETS and ITS2 cleavage (Michot et al., 1999; Peculis, 1997; Peculis and Steitz, 1993). The DEAD box helicase Ddx51 and the GTPase Nog1 have been implicated in 3′-ETS removal in murine cell lines, promoting U8 snoRNA release from the 5.8S-28S rRNA junction (Lapik et al., 2007; Srivastava et al., 2010)..

A genome-wide study of human RNA-binding proteins revealed unusual structural and expression characteristics for the RNA exonuclease REXO5/LOC81691, a metazoan-specific DEDDh 3′-5′ single-stranded RNA exonuclease (Gerstberger et al., 2014; Zuo and Deutscher, 2001). Rexo5 belong to the Rexo family in eukaryotes, known as Rex proteins in S. cerevisiae. While not functionally characterized in higher eukaryotes, S. cerevisiae Rex nucleases were shown to participate in rRNA and small nuclear RNAs (snRNAs) maturation (Faber et al., 2004; van Hoof et al., 2000).

Here, we report the genetic, molecular, and functional characterization of the D. melanogaster Rexo5 protein (CG8368) and document its requirement for 3′-exonucleolytic trimming of 28S rRNA, 5S rRNA, and snoRNAs. Rexo5 is essential for viability and loss-of-function results in nucleolar stress and ribosomal export defects. Furthermore, though Rexo5 and its mammalian homologs are ubiquitously expressed at low levels, their abundance is highly enriched in gonads, and high-level expression is essential for proper gonadal development in D. melanogaster.

RESULTS

Rexo5 is an evolutionary conserved, nucleolar and nuclear 3′-5′ RNA exonuclease

The Rexo5 exonuclease is unique to metazoans and distantly related to the REXO1/Rex1 family (Figure 2A). Vertebrate Rexo5 orthologs display a unique domain architecture of an RNase T domain paired with two RNA-recognition motifs (RRMs), which are absent in invertebrates (Figure 2B) (Finn et al., 2010). We obtained two Rexo5 loss-of-function mutants, $CG8368^{C04255}$ ($Rexo5^{PB}$) from the Harvard Exelixis collection harboring a transposon insertion, and $CG8368^{M100}$ ($Rexo5^{E497K}$) (Anderson et al., 1995), a glutamate-to-lysine E497K point mutant located in the RNase T domain, which we mapped through complementation tests (Figure 2C). $Rexo5^{PB}$ and $Rexo5^{E497K}$ homozygotes both exhibited lethality at second instar larval development (L2), while heterozygotes were fully viable and indistinguishable from wild-type controls. Protein and mRNA levels were depleted in $Rexo5^{PB}$, while $Rexo5^{E497K}$ showed normal expression of mRNA and elevated protein levels compared to wild-type, suggesting that $Rexo5^{E497K}$ did not impair protein translation, but resulted in direct or indirect loss of enzymatic activity of Rexo5 (Figure 2D). L2 lethality of both homozygous mutants could be rescued by Actin-GAL4 driven expression of the Rexo5 coding sequence, as well as by crossing it to two transgenic Rexo5 rescue lines, which included a 3.3 kb or 1.6 kb (disrupting zpg) endogenous promoter region (Figure 2C). Furthermore, Actin-GAL4-driven expression of alanine-substituted Rexo5 at one or two active site residues did not rescue lethality, demonstrating that the intact DEDDh catalytic site was required for viability (Figure S1C). Rexo5 protein and mRNA, ubiquitously expressed in all tissues, was highly elevated in adult gonads (Figure S1D–G). To investigate the subcellular localization of Rexo5 in vivo we generated transgenic flies expressing GFP-Rexo5 fusion protein from its endogenous promoter. GFP-Rexo5 was predominantly localized to the nucleolus and nucleus in somatic tissues (Figure 2E, S2G,H).

Rexo5 contains an RNase T-type nuclease domain composed of five catalytic residues (DEDDh): a general base histidine and four acidic catalytic residues (Asp-Glu-Asp-Asp), which chelate two Mg^{2+} ions, positioning a water molecule for nucleophilic attack at the scissile phosphodiester bond (Zuo and Deutscher, 2001). We recombinantly produced full-length wild-type ($Rexo5^{wt}$) and catalytically inactive ($Rexo5^{DADAH}$) mutant protein (Figure 2F), and measured nucleolytic activity for short, linear single-stranded RNA (ssRNA) and DNA (ssDNA), as well as circularized ssRNA (circRNA). $Rexo5^{wt}$ degraded linear ssRNA but not circRNA or ssDNA (Figure 2G, S2K–T). $Rexo5^{DADAH}$ exhibited no activity, indicating that the conserved DEDDh residues were required for biochemical activity. $Rexo5^{wt}$ preferentially cleaved oligoribocytidine and oligouridine over oligoriboadenosine

substrates (Figure S2L–Q). The enzymatic activity of Rexo5^{wt} was inhibited by EDTA, establishing a Mg^{2+}-dependent 3′-5′ RNA exonuclease activity. Human REXO5 was recently biochemically isolated and shown to have 3′-5′ specific ssRNA exonuclease activity in vitro, which was inhibited by 2′-O-methylation of the substrate 3′ end (Silva et al., 2017).

Rexo5 mutants exhibit global snoRNA processing defects

To investigate RNA targets of Rexo5 in vivo, we isolated total RNA from wild-type and homozygous mutant Rexo5 L2 larvae. At the latest viable time point, size and tissue morphologies of homozygous mutants were comparable to wild-type L2 larvae. Considering that RNAs in the nucleolus, the site of Rexo5 localization, range in size from less than 100 nucleotides (nt) for snoRNAs to thousands of nucleotide for rRNAs, we applied a small RNA sequencing protocol using partially hydrolyzed total RNA as input RNA (Gogakos et al., 2017). We analyzed each noncoding RNA group separately, first examining small abundant noncoding RNAs (20–200 nt), specifically snoRNAs, snRNAs (grouped into one category snoRNA/snRNA), and tRNAs (Figure 3A,C, S3A). To capture improperly processed RNAs we extended mature reference transcript sequences at the 5′ and 3′ end by 25 nt of genomic sequence and then calculated their overall transcript abundance. Transcript levels of snoRNAs were mildly elevated in mutants over wild-type controls, while tRNA expression levels were unaltered (Figure 3A,C). However, when inspecting the read density within the 25 nt window outside of the snoRNA/snRNA predicted 3′-termini, both mutants showed significant upregulation in snoRNAs, while tRNAs and snRNAs were unaffected and reads did not extend into the 3′-trailer region (Figure 3B,D). Coverage plots of selected snoRNAs, except for U3, revealed precursor accumulation extending 10–20 nt beyond the annotated snoRNA 3′-termini in both mutants (Rexo5^{PB} and Rexo5^{E497K}) (Figure 3E).

We independently confirmed the presence of 3′-trailer-comprising snoRNA precursors by Northern blot analysis for a subset of box C/D and H/ACA snoRNAs transcribed from separate promoters (independent), as snoRNA-cistrons (cistronic), or located within mRNA introns (intronic) (Figure 3F). Loss of Rexo5 lead to accumulation of incompletely matured snoRNAs in a broader second band migrating 10–20 nt above the mature snoRNA size in homozygous mutants (Figure 3F). Independently transcribed U3 snoRNA showed no precursor accumulation in agreement with RNA-seq analysis, whereas U8 snoRNA, located at the predicted snoRNA:185 locus ((Peculis, 1997) and B. Peculis personal comm.), accumulated a 3′ trailer. ~50% of each snoRNA accumulated as incompletely 3′-trimmed precursors by Northern Blot quantification (Figure S3C).

To determine the number of 3′ residual nucleotides on snoRNA precursors in homozygous mutants, we analyzed six biological replicate hydrolysis-based small RNA-seq datasets (averaging three Rexo5^{PB} and three Rexo5^{E497K} datasets) and compared them to four wild-type replicates, requiring ≥2 read counts spanning the 3′-region (Figure 3G, S4). Out of 155 expressed snoRNAs 112 (70%) retained 3′ tails of ≥5 nt length (89 with $p \leq 0.05$) (Figure 3G, category 1, Table S1). Few highly abundant snoRNAs also showed read coverage of ≥2 reads in their 3′ precursors in wild-type controls, hence their true 3′-extensions are hidden in Figure 3G (category 2). Neither snRNAs (Figure 3B,G, category 3), nor tRNAs (Figure

3C,D, S4) were affected in processing or abundance in mutants, indicating that Rexo5 processing activity is specific for snoRNAs.

Rexo5 mutants accumulate 3′-unprocessed 5S rRNAs

Alignment of reads from hydrolysis-based RNA-seq data to 5S rRNA genes revealed a 100-fold accumulation of 5S rRNA precursors in homozygous L2 mutant larvae over wild-type controls (Figure 4A, Log2 Diff plot). Furthermore, mature 5S rRNAs were aberrantly misprocessed, retaining a 3-nt 3′ trailer in homozygous mutants otherwise absent in wild-type larvae (Figure 4A). The aberrant 5S rRNAs co-migrated at the level of mature 5.8S rRNA, visualized by ethidium bromide staining of polyacrylamide gels (Figure 4B). In vivo Tubulin-GAL4-driven shRNA knockdowns of Rexo5 accumulated similarly misprocessed 5S rRNAs (Figure 4B). This suggested that Rexo5 is the primary nuclease responsible for 5S rRNA 3′-trimming in D. melanogaster.

Northern blot analysis confirmed the shift of 5S rRNA in homozygous mutants, while 5.8S rRNA remained unaltered, and accumulated unprocessed 5S rRNA precursors (Figure 4C). The longer mature 5S rRNA in Rexo5 homozygous mutants mirrored the processing defects observed in S. cerevisiae Rex1p deletion strains, which accumulate 5S rRNAs retaining 10 nt of their precursor sequence at the 3′ end (Piper et al., 1983). Together, the data demonstrate that removal of the 3′ trailer and correct formation of mature 5S rRNA 3′ ends requires Rexo5.

Rexo5 mutants accumulate 3′-end-misprocessed 28S rRNA precursors

Alignment of hydrolysis-based RNA-seq reads to the 47S rDNA showed increased read coverage in the 3′-ETS/intergenic region for homozygous mutants compared to wild-type controls (Figure 5A, S3A). The D. melanogaster rDNA transcript M2017.1 (GenBank ID) spans the 7.2 kb (18S, 5.8S, and 28S comprising) rRNA precursor, as well as a 4.5 kb intergenic region, reaching the 18S rRNA sequence of the adjacent rDNA locus (Figure 5A). Read coverage plots across M2017.1 showed that reads covered the entire intergenic region in homozygous mutants, with the majority mapping to a 200-nt window immediately downstream of the mature 28S 3′ end (Figure 5A upper panel). Assessment of the fold-change differences in RNA-seq coverage of the 3′-ETS in homozygous mutants and wild-type controls revealed a 1000-fold increase (Figure 5A lower panel). Illumina TruSeq total RNA-seq, limited to detection of input RNAs longer than 200 nt, confirmed this observation (Figure 5B, S3B).

3′-ETS processing defects were further supported by Northern blot analysis comparing L2 homozygous Rexo5^{PB} and Rexo5^{E497K} mutant larvae with heterozygotes and wild-type controls. RNA from homozygous mutants revealed two distinct bands when probed for the 3′-ETS: one band at 2.5 kb, slightly shifted above the mature 28Sb rRNA (product c′, Figure 5C,D), and a second band at 5–8 kb, ranging from the rRNA precursor intermediate b′ (at 4.7 kb, containing ITS1, 5.8S, ITS2, and 28S) to the full-length 47S rRNA precursor (pre-rRNA) (Figure 5C,D, S5A–D) (Long and Dawid, 1980). Heterozygotes and wild-type controls showed no hybridization signal for the 3′-ETS, confirming that under steady state conditions the 3′-ETS was already trimmed (Figure 5D). Furthermore, accumulation of the

ITS1 was observed specifically in homozygous Rexo5^{E497K} mutants by Northern blot analysis, but was absent in Rexo5^{PB}. While Rexo5^{PB} larvae were devoid of Rexo5 protein, Rexo5^{E497K} showed significantly increased protein levels (Figure 2D). It is conceivable that nonfunctional Rexo5^{E497K} mutant protein still binds to the ITS1 and interferes with efficient downstream processing, leading to accumulation of intermediate b.

The 3′-ETS hybridization signal was stronger for Rexo5^{PB} compared to Rexo5^{E497K} homozygotes, mirroring the higher fold-change difference of unprocessed 3′-ETS in Rexo5^{PB} compared to Rexo5^{E497K} homozygous mutants observed by RNA-seq. Rexo5 homozygous mutants accumulated a continuous size range of pre-rRNA intermediates, encompassing the full-length pre-rRNA, 3′-end-misprocessed 45S, 43S, 32S intermediates, and the 3′-misprocessed 28Sb rRNA, suggesting that the 3′-ETS is indeed subject to exonucleolytic processing.

To quantify accumulation of 3′-ETS-containing rRNA precursors in Rexo5 mutants in hydrolysis-based and total RNA-seq datasets, we determined the number of reads mapping to a 200-nt window immediately downstream of the 28S rRNA 3′ end and normalized it to the read count of a 200-nt window within ITS2. The percentage of pre-rRNAs sequenced by total RNA-seq showed large variability as size selection caused low ITS2 and ITS1 and a higher 3′-ETS coverage, which falsely skewed the ratios. Quantification of hydrolysis-based RNA-seq data showed that up to 40% of pre-rRNA intermediates contained unprocessed 3′-ETS in Rexo5 homozygous mutants compared to 0–3% in wild type larvae (Figure S3D).

The *D. melanogaster* Ddx51 homolog Dbp73D has a conserved function in 3′-ETS removal

The D. melanogaster helicase Dbp73D is the conserved ortholog of mammalian Ddx51 implicated in 28S rRNA 3′ end maturation in mice (Srivastava et al., 2010). Tubulin-GAL4-driven shRNA knockdowns of Dbp73D and Rexo5 were both lethal at the L2 developmental stage. Total RNA-seq of Dbp73D shRNA knockdowns also revealed accumulation of reads in the 3′-ETS (Figure 5E). 3′-ETS-containing pre-rRNAs were 100-fold enriched in Dbp73D knockdowns, 10-fold less than the ~1000-fold 3′-ETS enrichment seen in Rexo5 knockdowns. shRNA knockdowns of other rRNA biogenesis factors involved in distinct pre-rRNA processing events in the 5′-ETS (nop5, human NOP58), ITS1 (CG6937, NFIK), and ITS2 (CG5033, BOP1) showed no effect on the 3′-ETS (Figure 5E, S5). Knockdown of 3′-5′ ssRNA exonucleases, including the RNA exosome nucleases Rrp6 (EXOSC10) and Dis3 (DIS3), and the DEDDh RNA exonuclease CG6833 (REXO4), as well as a homozygous genetic mutant of CG12877 (CG12877^{e00300}, REXO1), did not accumulate 3′-ETS-containing pre-rRNAs (Figure 5F, S5). All UAS-shRNA Tubulin-GAL4 knockdowns tested were lethal at L1 or L2 larval stage displaying 2- to 17-fold target mRNA repression (Figure S5E,F). shRNA knockdowns of other Rexo family members were not lethal and therefore not further investigated.

Northern blot analysis probing against the 3′-ETS in Dbp73D knockdowns revealed accumulation of precursors in size between 32S and 47S pre-rRNA (Figure 5G). However, in contrast to Rexo5 shRNA knockdowns and Rexo5 homozygous mutants, Dbp73D knockdowns showed no accumulation of the ~2.5 kb band at the migration size of mature 28Sb rRNA (Figure 5G). While rRNA biogenesis in Rexo5 loss-of-function mutants

continued to form 28Sb rRNA, rRNA processing halted earlier at intermediate b in Dpb73D knockdowns. These results confirmed a functionally conserved role of Dbp73D and mammalian Ddx51 in 28S rRNA 3′ end maturation. The distinct processing patterns of Dpb73D and Rexo5 mutants suggest that Dbp73D and Rexo5 act at different steps during 3′-ETS removal.

Rexo5 mutants exhibit ribosomal export defects

A genome-wide RNAi screen for regulators of nucleolar size in S2 cells noted a 2-fold nucleolar increase in Rexo5 knockdown cells (Neumuller et al., 2013). Similarly, we also observed increased nucleolar size in midgut cells when compared to wild-type or heterozygous L2 larvae (Figure S6N,O). For side-by-side comparisons of cells from the same tissue we employed clonal expression of transgenic Rexo5 shRNA under the hsFlp-Tubulin-GAL4 driver and examined nucleolar differences of RNAi clones compared to wild-type cells in the gut at the L3 larval stage (Figure 6A–A″, S6P,Q). Rexo5 knockdowns showed a 4-fold increase of nucleolar size compared to wild-type cells, indicative of increased ribosomal nucleolar stress (Figure 6A′″) (Boulon et al., 2010; Nicolas et al., 2016).

We carried out RNA fluorescence in situ hybridization (RNA-FISH) on hetero-and homozygous Rexo5 mutant larvae with a probe against a 34-nt repeat that is interspersed seven times within the 3′-ETS. As expected, only homozygous mutants showed fluorescent signals, which was exclusively confined to the nucleolus (Figure 6B–G,B″–G″). These results demonstrated that unprocessed 3′-ETS-containing 28S rRNA precursors were not exported to the cytosol. We then probed mature 28S rRNA, which predominantly localized to the cytosol (Figure 6B,C), and mature 18S rRNA, which unexpectedly was retained and accumulated in the nucleolus of homozygous mutants (Figure 6D,E).

To assess whether loss-of-function of Rexo5 affected small subunit export at the protein level, we compared the localization of GFP-tagged ribosomal proteins RpS2-GFP and RpL13A-GFP in $Rexo5^{PB}$ and $Rexo5^{E497K}$ mutants in vivo. While in heterozygous mutants RpS2-GFP predominantly localized to the cytoplasm, RpS2-GFP accumulated in the nucleolus of homozygous mutants (Figure 6F,G, S6). Only few cells were captured with noticeable nuclear retention in homozygous Rexo5 RpL13A-GFP mutants, while the majority displayed unaltered, predominantly cytoplasmic localization of RpL13A–GFP (Figure S6E,F). To verify this observation we assessed the localization of UAS-RFP-RpL26 in Rexo5 and Dbp73D shRNA knockdowns under the Tubulin-GAL4 driver. Knockdown of both genes showed, if any effect, only weak nuclear accumulation (~10%) of RFP-RpL26 compared to the white shRNA knockdown control (Figure S6K–M).

Rexo5 is required for gonadal development

Levels of rRNA biogenesis factors and specific upregulation of nucleolar size and rRNA transcription are known to impact stem cell differentiation and maintenance in germline development (Neumüller et al., 2008; Sanchez et al., 2016; Q. Zhang et al., 2014). We had noted high enrichment of Rexo5 in both male and female gonads by in vivo localization of GFP-Rexo5 and Western blot analysis of endogenous Rexo5 (Figure 7A–D, S1H, S2A–F).

In testes, GFP-Rexo5 localized to the nuclei of mitotic cells and during sperm terminal differentiation to the cytoplasm, concentrating at the front end of actin cones in the cystic bulge (Figure 7A–C, S2D–E) (Noguchi and K. G. Miller, 2003). In ovaries, Rexo5 was highly abundant, localizing to nuclei of follicle and nurse cells, and the oocyte nucleus (Figure 7D, S2F).

We next assessed developmental progression of male and female gonads in Rexo5 mutants. We first assessed the development of male gonads during L2 in Rexo5 homozygous mutants, the last point before organismal death. While female gonadal development starts later, male germline development initiates during embryogenesis and at the end of L2 larval development testes undergo all four rounds of mitotic divisions (Figure 7E) (Sheng et al., 2009). At L2, wild-type male gonialblasts had reached four mitotic divisions and formed the 16-cell cyst (Figure 7F). In contrast, gonads of Rexo5 homozygous L2 mutants were ~10-fold smaller in size compared to wild-type, had fewer cells, and gonialblast divisions were arrested at the first or second mitotic division, assessed by the level of branching of connected fusomes in mitotic cells (Figure 7G).

To study gonadal developmental defects in adult flies, we rescued the early lethality of Rexo5 mutants in somatic cells expressing transgenic UAS-Rexo5 under the Actin-GAL4 driver. The pUASt-GAL4 expression system works inefficiently in the Drosophila germline (Brand and Perrimon, 1993; Rorth, 1998), which allowed us to overexpress Rexo5 in somatic cells but not germline stem cells (GSCs) and differentiated progenitors in the genetic mutant background. Loss-of-function of Rexo5 in the testes of adult males 3-days and 14-days post eclosion resulted in spermatogonial cells that failed to differentiate properly. Instead of being confined to the mitotic area in testes, multicellular germ cell cysts with branched fusomes were distributed throughout the entire testicular tube in Rexo5 mutants (Figure 7H,I, S7C–E). At 3 days, mutant germ cells did not progress into meiosis, detected by the absence of serine 10 phosphorylated histone H3 (PH3) (Figure 7J,K) (Wei et al., 1998). Knockdown of Rexo5 using the nanos GAL4 (nos-GAL4) driver resulted in weaker germline defects. 3-day-old nos-GAL4 shRNA-Rexo5 testes appeared morphologically indistinguishable to wild-type, but meiotic nuclei were absent in shRNA-Rexo5 testes at 14 days ($p<0.01$ Fisher exact test, Figure S7I,J). The lower penetration of the phenotype may be attributable to incomplete RNAi repression by the nanos driver, as expression levels of nanos are 100-fold lower than Rexo5 (modENCODE).

Finally, adult Actin-GAL4-rescued mutant testes showed increased genomic instability, displaying elevated levels of H2Av phosphorylation indicative of increased double-stranded DNA (dsDNA) breaks (Figure 7L–N) (Madigan et al., 2002). In agreement with this observation, mRNA levels of Ku70/80 and MRN complex components of the dsDNA non-homologous end joining (NHEJ) repair pathway were also >4-fold upregulated in L2 homozygous mutants (Figure S7K–M).

Actin-GAL4 pUASt-Rexo5 rescued homozygous mutant females were sterile and had rudimentarily developed ovaries, resembling the string-of-pearls phenotype described for RpS2 mutants (Figure 7P) (Cramton and Laski, 1994). Mutant oocytes did not fully develop and displayed egg-chamber degeneration at stage 4–6 of oocyte development, leading to

homozygous females having >10-fold smaller ovaries. Near-complete loss of GSCs and germarium proliferation defects were observed after 14 days (Figure 7Q, S7B). nos-GAL4 knockdowns of Rexo5 resulted in smaller, growth-degenerate ovaries and ~50% of germaria exhibited proliferation defects at 3 days (Figure S7F–H). These observations agreed with the phenotypes isolated for Rexo5 in a previous genome-wide RNAi screen of female germline stem cell regulators (Sanchez et al., 2016). Like L2 larvae, mutant ovaries and testes of Actin-GAL4 rescued adult flies also accumulated 3′-ETS containing 28S rRNA precursors by RNA-seq (Figure S5O), explaining the characteristic ribosomal gene defect phenotype observed for mutant ovaries.

We analyzed mRNA-seq data from tissue atlas projects for D. melanogaster, human, and murine Rexo5 homologs, which showed that the high expression of Rexo5 in adult testes was conserved across all three species (Figure S1G). At the mRNA level, human REXO5 was among the most tissue-specifically expressed genes, its abundance among the top 100 expressed genes in testes. The elevated expression of Rexo5 was unique among RNA exonucleases, specifically for DEDDh RNase T class exonucleases (Figure S1D), and it was unique for any established ribosome biogenesis factor, possibly suggesting an additional conserved role of Rexo5 in gonads beyond rRNA and snoRNA maturation. While Rexo5 showed peak expression during terminal differentiation and elongation of spermatids, our data demonstrated that already during early germline development Rexo5 is critical for meiotic entry, cell growth, and proliferation in male and female gonads.

DISCUSSION

Transcriptome-wide characterization of Rexo5 endogenous RNA targets using small RNA-seq methods

Genome-wide investigation of RNases in higher eukaryotes is an active area of research (Chang et al., 2013; Schneider et al., 2012), but the targets of the majority of the ~160 RNases in higher eukaryotes remain unknown (Gerstberger et al., 2014). Here we show that the 3′-5′ RNase T class exonuclease Rexo5 is an essential protein in D. melanogaster and functions in the exonucleolytic maturation of the 3′-termini of snoRNAs, 5S and 28S rRNAs. We applied a hydrolysis-based small RNA-sequencing protocol to monitor all cellular RNAs, including the size range of 50–200 nt otherwise not covered by conventional methods, and identified the RNA targets of a previously uncharacterized nuclease. Our approach revealed transcriptome-wide 3′ end processing defects of 3–20 nt and is generally applicable for the characterization of RNases implicated in RNA processing and turnover in higher eukaryotes.

Rexo5 is a novel 3′-nucleolytic factor in eukaryotic snoRNA maturation

In S. cerevisiae, nuclear 5′-3′ exonuclease Xrn2/Rat1p and RNA exosome 3′-5′ exonuclease Rrp6, carry out 5′ and 3′ end snoRNA maturation, respectively (Allmang et al., 1999; Petfalski et al., 1998). Recent data suggests, however, that the role of Rrp6 in 3′ end snoRNA is not conserved and Rrp6 (EXOSC10) only plays a minor role in snoRNA biogenesis in higher eukaryotes (Berndt et al., 2012; Lubas et al., 2015). Instead, Rrp6, recruited by RBM7 and DGCR8, executes turnover of nascent RNAs and snoRNAs (Lubas

et al., 2015; Macias et al., 2015). Polyadenylation followed by poly(A)-specific ribonuclease (PARN) processing was shown to mature some H/ACA snoRNAs and telomerase RNA in humans (Berndt et al., 2012; Moon et al., 2015).

We find that Rexo5 plays a prominent role in C/D and H/ACA snoRNA 3′ end processing and mutants of Rexo5 accumulate snoRNA precursors. Precursor accumulation is not complete, which may suggest that alternative, less effective snoRNA maturation pathways, such as polyadenylation and PARN processing (Berndt et al., 2012), come into play in the absence of Rexo5.

Rexo5 selectively processes the 3′ ends of 5S and 28S rRNA precursors

The 3′-5′ DEDDh RNA exonuclease Eri1, the RNA exosome, and the RNA endonuclease Nob1 have previously been shown in 3′ end processing of 5.8S rRNA and 18S rRNA (Ansel et al., 2008; Briggs et al., 1998; Gabel and Ruvkun, 2008; Pertschy et al., 2009; Preti et al., 2013; Sloan et al., 2013). In S. cerevisiae, exonucleolytic trimming of 5S and 28S rRNAs is executed by Rex1p (Kempers-Veenstra et al., 1986; Piper et al., 1983). Here we show that Rexo5, a newly evolved nuclease distantly related to the Rexo1 subfamily, is the primary enzyme involved in 3′ end processing of 5S and 28S rRNAs in D. melanogaster. Rex1p has two possible orthologs in the Rexo1 subfamily in D. melanogaster, CG12877 and CG42666, distinct from Rexo5. Analysis of the genetic $CG12877^{e00300}$ mutant, lethal at L1 (Figure S5), revealed no accumulation of rRNA or snoRNA precursors. In vivo knockdowns and genetic mutants of CG42666 (prage), implicated in destabilization of maternal mRNAs during embryogenesis, are viable (Cui et al., 2016; Liu et al., 2016; Tadros et al., 2003), suggesting that prage is not an essential regulator of cell survival. Considering that Rexo1 homologs are expressed at comparable levels to Rexo5 in somatic tissues, but were unable to compensate for loss-of-function of Rexo5, we conclude that a redundant role of these nucleases is unlikely.

We show the functional conservation of Dbp73D, ortholog of mammalian Ddx51 helicase, in U8-dependent 28S rRNA 3′ end maturation in D. melanogaster. Further supporting a conserved role of Rexo5 in metazoan rRNA biogenesis, human REXO5 also exhibits nucleolar localization and RNA exonuclease activity (Figure S2J) (Silva et al., 2017). Future investigation of the vertebrate Rexo5 homologs, as well as other Rexo family members, will clarify their role in nuclear maturation of rRNAs.

Despite the evolution of additional factors in 3′ end maturation in higher eukaryotes including U8 snoRNA, 3′ exonucleolytic processing of 28S rRNA remained conserved between S. cerevisiae and D. melanogaster. This revises our understanding of how the 47S rRNA precursor may mature in higher eukaryotes. Instead of guiding the proposed precise endonucleolytic cleavage reaction at the 28S 3′ end, basepairing of U8 snoRNA with 47S pre-rRNA may function to expose and thereby present the 3′ end of 28S rRNA for exonucleolytic trimming. Indeed, earlier studies in X. laevis proposed that downstream endonucleolytic cleavage at T2 was followed by rapid exonucleolytic trimming to the 3′ end of 28S rRNA (T1), generating the 40S precursor (Labhart and Reeder, 1986). Overall, an exonucleolytic mechanism may also explain the lack of conservation and the observed sequence heterogeneity of 3′-ETS sequences across organisms (Mandal and Dawid, 1981).

Rexo5 affects ribosome assembly, nucleolar size and genome integrity

Rexo5 mutants exhibit increased nucleolar size, indicative of nucleolar stress (Boulon et al., 2010), and show nuclear retention of the 40S ribosomal subunit. Rexo5 processes 28S and 5S rRNA - both RNAs of the 60S subunit. Hence, small subunit export defects must be attributable to an indirect, secondary effect of dysfunctional or limited specific snoRNPs required for 18S rRNA modification, RNA folding, or ribosomal protein assembly. Alternatively, the different localizations may be due to different assembly and transport rates of the two ribosomal subunits. Small and large ribosomal subunits are exported to the cytosol by two distinct pathways and the 40S small subunit, undergoing fewer maturation steps, is more rapidly exported than the 60S subunit (Udem and Warner, 1973; Zemp and Kutay, 2007). Nuclear retention of the small ribosomal subunit may simply be due to different rates of small versus large ribosomal subunit export for which mature snoRNP levels become rate-limiting.

Dysregulation of rRNA and snoRNA maturation pathways in Rexo5 mutants affected genomic stability leading to increased levels of dsDNA breaks and upregulation the NHEJ repair pathway. These may point to either an additional role of Rexo5 in NHEJ repair or could be a consequence of general RNA processing defects or nucleolar stress leading to overall genomic instability (Boulon et al., 2010; Wickramasinghe and Venkitaraman, 2016).

Roles of Rexo5 in germline differentiation and gonadal development

Lastly, high levels of Rexo5 are critical for germline differentiation. Consistent with our observations, two recent genome-wide RNAi screens observed rudimentary ovarian morphology and early differentiation/germarium defects for Rexo5 knockdowns (Handler et al., 2013; Sanchez et al., 2016).

The germline-specific upregulation of an RNA exonuclease involved in rRNA biogenesis is unparalleled by other rRNA biogenesis genes (Gerstberger et al., 2014). Tailoring translational efficiencies of ribosomes through tissue-specific incorporation of ribosomal proteins (Kondrashov et al., 2011; Vesper et al., 2011; X. Zhang et al., 2015) and cell-type specific heterogeneity of rRNA modifications, precursor ratios and mature rRNA isoforms (such as $5.8S_S$ and $5.8S_L$) were previously reported (Lafontaine, 2015; Mullineux and Lafontaine, 2012). Tissue-specific expression of an rRNA biogenesis factor, however, is not commonly observed and may indicate tissue-specific tailoring of rRNA biogenesis to promote alternative rRNA biogenesis pathways. In addition, the extremely high expression levels in D. melanogaster, humans and mice, as well as the cytoplasmic localization of Rexo5 at the individualization complexes may point to a specific role of Rexo5 during late sperm maturation. It is conceivable that Rexo5 has a dual function in rRNA biogenesis and during late spermatogenesis, either in the removal of paternal RNA or in the processing of noncoding RNAs that are zygotically transferred (Rassoulzadegan et al., 2006).

In summary, this study discovered a novel and essential snoRNA and rRNA 3′-end-processing enzyme and detailed its molecular function in vivo using a combination of RNA-seq and traditional Northern blotting approaches. This strategy is generally applicable to the

study of many orphan target ribonucleases encoded in eukaryotes and their respective roles in coding and non-coding RNA biogenesis and turnover.

EXPERIMENTAL PROCEDURES

A detailed version of the experimental procedures can be found in the Supplemental Information.

Fly Stocks and Husbandry

All crosses were performed at 22–25°C. The *D. melanogaster* sequencing strain was used as control. Detailed stock information and cloning procedures for all transgenic lines are given in the supplemental information.

Clonal analysis of RNAi clones

UAS-shRNA-Rexo5/Cyo; Sb/TM6B males were crossed to yw hsFlp;Sco/Cyo;UAS#Red47a#1tub<+GFP<GAL4/TM6B females, and embryos were heat shocked after 24 h egg laying at 37°C for 1 h. Non-TM6B L3 larvae were dissected and processed for immunofluorescence. Nucleolar/nuclear size ratios were measured using ImageJ.

In vivo shRNA knockdowns

UAS-shRNAs fly lines were crossed to Sp/Cyo;Tubulin-GAL4/TM6B and UAS-GFP-RpL26;;Tubulin-GAL4/TM6B, larvae were collected for immunofluorescent stainings, RNA-FISH, or RNA isolation for RNA-sequencing.

RNA-seq methods

Whole larvae and PBS-dissected gonads were directly homogenized in TRIzol with a 1 ml tissue grinder and total RNA isolated according to the manufacturer's protocol. poly(A) mRNA purification and total RNA cDNA library construction was performed using the TruSeq version 1.5 kit (Illumina). cDNA was barcoded using the Illumina Multiplexing Sample Preparation Oligonucleotide kit and analyzed on an Illumina HiSeq2000 in a 100-base-pair (bp) single-end sequencing run. Hydrolysis-based small RNA-seq was performed as described in the supplemental information. All RNA-sequencing data is deposited on the NCBI SRA repository under the bioproject ID PRJNA373931.

Supplementary Material

Refer to Web version on PubMed Central for supplementary material.

Acknowledgments

We thank Z. Ozair, A. Garzia, M. Mazzola, M. Hafner, and Y. Gultekin for careful reading of the manuscript. We thank all members of the Tuschl and Steller laboratories, B. Peculis for discussions on U8 snoRNA, A. Spradling and P. DiMario for their generous donations of fly stocks, M. Ascano for recombinant Translin-Trax. S.G. was supported by the Boehringer Ingelheim Fonds Fellowship and the TPCB Program. Part of this work was supported by NIH grant RO1GM60124 to H.S.

References

Allmang C, Kufel J, Chanfreau G, Mitchell P, Petfalski E, Tollervey D. Functions of the exosome in rRNA, snoRNA and snRNA synthesis. EMBO J. 1999; 18:5399–5410. [PubMed: 10508172]

Anderson MG, Perkins GL, Chittick P, Shrigley RJ, Johnson WA. drifter, a Drosophila POU-domain transcription factor, is required for correct differentiation and migration of tracheal cells and midline glia. Genes Dev. 1995; 9:123–137. [PubMed: 7828848]

Ansel KM, Pastor WA, Rath N, Lapan AD, Glasmacher E, Wolf C, Smith LC, Papadopoulou N, Lamperti ED, Tahiliani M, Ellwart JW, Shi Y, Kremmer E, Rao A, Heissmeyer V. Mouse Eri1 interacts with the ribosome and catalyzes 5.8S rRNA processing. Nat. Struct. Mol. Biol. 2008; 15:523–530. [PubMed: 18438418]

Berndt H, Harnisch C, Rammelt C, Stöhr N, Zirkel A, Dohm JC, Himmelbauer H, Tavanez J-P, Hüttelmaier S, Wahle E. Maturation of mammalian H/ACA box snoRNAs: PAPD5-dependent adenylation and PARN-dependent trimming. RNA. 2012; 18:958–972. [PubMed: 22442037]

Boulon S, Westman BJ, Hutten S, Boisvert F-M, Lamond AI. The Nucleolus under Stress. Mol. Cell. 2010; 40:216–227. [PubMed: 20965417]

Brand AH, Perrimon N. Targeted gene expression as a means of altering cell fates and generating dominant phenotypes. Development. 1993; 118:401–415. [PubMed: 8223268]

Briggs MW, Burkard KT, Butler JS. Rrp6p, the yeast homologue of the human PM-Scl 100-kDa autoantigen, is essential for efficient 5.8 S rRNA 3′ end formation. J. Biol. Chem. 1998; 273:13255–13263. [PubMed: 9582370]

Chang H-M, Triboulet R, Thornton JE, Gregory RI. A role for the Perlman syndrome exonuclease Dis3l2 in the Lin28-let-7 pathway. Nature. 2013; 497:244–248. [PubMed: 23594738]

Chong MMW, Rasmussen JP, Rudensky AY, Rundensky AY, Littman DR. The RNAseIII enzyme Drosha is critical in T cells for preventing lethal inflammatory disease. J. Exp. Med. 2008; 205:2005–2017. [PubMed: 18725527]

Ciganda M, Williams N. Eukaryotic 5S rRNA biogenesis. WIREs RNA. 2011; 2:523–533. [PubMed: 21957041]

Cramton SE, Laski FA. string of pearls encodes Drosophila ribosomal protein S2, has Minute-like characteristics, and is required during oogenesis. Genetics. 1994; 137:1039–1048. [PubMed: 7982558]

Cui J, Lai YW, Sartain CV, Zuckerman RM, Wolfner MF. The Drosophila prage Gene, Required for Maternal Transcript Destabilization in Embryos, Encodes a Predicted RNA Exonuclease. G3 (Bethesda). 2016; 6:1687–1693. [PubMed: 27172196]

Elela SA, Igel H, Ares M. RNase III cleaves eukaryotic preribosomal RNA at a U3 snoRNP-dependent site. Cell. 1996; 85:115–124. [PubMed: 8620530]

Faber AW, Vos JC, Vos HR, Ghazal G, Elela SA, Raué HA. The RNA catabolic enzymes Rex4p, Rnt1p, and Dbr1p show genetic interaction with transacting factors involved in processing of ITS1 in Saccharomyces cerevisiae pre-rRNA. RNA. 2004; 10:1946–1956. [PubMed: 15525710]

Finn RD, Mistry J, Tate J, Coggill P, Heger A, Pollington JE, Gavin OL, Gunasekaran P, Ceric G, Forslund K, Holm L, Sonnhammer ELL, Eddy SR, Bateman A. The Pfam protein families database. Nucleic Acids Res. 2010; 38:D211–D222. [PubMed: 19920124]

Gabel HW, Ruvkun G. The exonuclease ERI-1 has a conserved dual role in 5.8S rRNA processing and RNAi. Nat. Struct. Mol. Biol. 2008; 15:531–533. [PubMed: 18438419]

Gerstberger S, Hafner M, Tuschl T. A census of human RNA-binding proteins. Nat. Rev. Genet. 2014; 15:829–845. [PubMed: 25365966]

Gogakos T, Brown M, Garzia A, Meyer C, Hafner M, Tuschl T. Characterizing Expression and Processing of Precursor and Mature Human tRNAs by Hydro-tRNAseq and PAR-CLIP. Cell Rep. 2017; 20:1463–1475. [PubMed: 28793268]

Gurney T. Characterization of mouse 45S ribosomal RNA subspecies suggests that the first processing cleavage occurs 600 +/− 100 nucleotides from the 5” end and the second 500 +/− 100 nucleotides from the 3” end of a 13.9 kb precursor. Nucleic Acids Res. 1985; 13:4905–4919. [PubMed: 4022778]

Handler D, Meixner K, Pizka M, Lauss K, Schmied C, Gruber FS, Brennecke J. The genetic makeup of the Drosophila piRNA pathway. Mol. Cell. 2013; 50:762–777. [PubMed: 23665231]

Henras AK, Plisson-Chastang C, O′Donohue M-F, Chakraborty A, Gleizes P-E. An overview of pre-ribosomal RNA processing in eukaryotes. WIREs RNA. 2014; 6:225–242. [PubMed: 25346433]

Jordan BR. Demonstration of intact 26 S ribosomal RNA molecules in Drosophila cells. J. Mol. Biol. 1975; 98:277–280. [PubMed: 1195384]

Kempers-Veenstra AE, Oliemans J, Offenberg H, Dekker AF, Piper PW, Planta RJ, Klootwijk J. 3′-End formation of transcripts from the yeast rRNA operon. EMBO J. 1986; 5:2703–2710. [PubMed: 3780675]

Kondrashov N, Pusic A, Stumpf CR, Shimizu K, Hsieh AC, Xue S, Ishijima J, Shiroishi T, Barna M. Ribosome-Mediated Specificity in Hox mRNA Translation and Vertebrate Tissue Patterning. Cell. 2011; 145:383–397. [PubMed: 21529712]

Kressler D, Linder P, la Cruz de J. Protein trans-acting factors involved in ribosome biogenesis in Saccharomyces cerevisiae. Mol. Cell. Biol. 1999; 19:7897–7912. [PubMed: 10567516]

Kufel J, Dichtl B, Tollervey D. Yeast Rnt1p is required for cleavage of the pre-ribosomal RNA in the 3′ ETS but not the 5′ ETS. RNA. 1999; 5:909–917. [PubMed: 10411134]

Kuhn A, Grummt I. 3′-end formation of mouse pre-rRNA involves both transcription termination and a specific processing reaction. Genes Dev. 1989; 3:224–231. [PubMed: 2714650]

Labhart P, Reeder RH. A 12-base-pair sequence is an essential element of the ribosomal gene terminator in Xenopus laevis. Mol. Cell. Biol. 1987; 7:1900–1905. [PubMed: 3600650]

Labhart P, Reeder RH. Characterization of three sites of RNA 3′ end formation in the Xenopus ribosomal gene spacer. Cell. 1986; 45:431–443. [PubMed: 3453104]

Lafontaine DLJ. Noncoding RNAs in eukaryotic ribosome biogenesis and function. Nat. Struct. Mol. Biol. 2015; 22:11–19. [PubMed: 25565028]

Lapik YR, Misra JM, Lau LF, Pestov DG. Restricting conformational flexibility of the switch II region creates a dominant-inhibitory phenotype in Obg GTPase Nog1. Mol. Cell. Biol. 2007; 27:7735–7744. [PubMed: 17785438]

Lee Y, Ahn C, Han JJ, Choi H, Kim J, Yim J, Lee J, Provost P, Radmark O, Kim S, Kim VN. The nuclear RNase III Drosha initiates microRNA processing. Nature. 2003; 425:415–419. [PubMed: 14508493]

Liu Y, Ge Q, Chan B, Liu H, Singh SR, Manley J, Lee J, Weideman AM, Hou G, Hou SX. Whole-animal genome-wide RNAi screen identifies networks regulating male germline stem cells in Drosophila. Nat. Commun. 2016; 7:12149. [PubMed: 27484291]

Long EO, Dawid IB. Alternative pathways in the processing of ribosomal RNA precursor in Drosophila melanogaster. J. Mol. Biol. 1980; 138:873–878. [PubMed: 6774101]

Lubas M, Andersen PR, Schein A, Dziembowski A, Kudla G, Jensen TH. The human nuclear exosome targeting complex is loaded onto newly synthesized RNA to direct early ribonucleolysis. Cell Rep. 2015; 10:178–192. [PubMed: 25578728]

Macias S, Cordiner RA, Gautier P, Plass M, Cáceres JF. DGCR8 Acts as an Adaptor for the Exosome Complex to Degrade Double-Stranded Structured RNAs. Mol. Cell. 2015; 60:873–885. [PubMed: 26687677]

Madigan JP, Chotkowski HL, Glaser RL. DNA double-strand break-induced phosphorylation of Drosophila histone variant H2Av helps prevent radiation-induced apoptosis. Nucleic Acids Res. 2002; 30:3698–3705. [PubMed: 12202754]

Mandal RK, Dawid IB. The nucleotide sequence at the transcription termination site of ribosomal RNA in Drosophila melanogaster. Nucleic Acids Res. 1981; 9:1801–1811. [PubMed: 6264393]

Michot B, Joseph N, Mazan S, Bachellerie JP. Evolutionarily conserved structural features in the ITS2 of mammalian pre-rRNAs and potential interactions with the snoRNA U8 detected by comparative analysis of new mouse sequences. Nucleic Acids Res. 1999; 27:2271–2282. [PubMed: 10325414]

Miller OL, Beatty BR. Visualization of nucleolar genes. Science. 1969; 164:955–957. [PubMed: 5813982]

Moon DH, Segal M, Boyraz B, Guinan E, Hofmann I, Cahan P, Tai AK, Agarwal S. Poly(A)-specific ribonuclease (PARN) mediates 3′-end maturation of the telomerase RNA component. Nat. Genet. 2015; 47:1482–1488. [PubMed: 26482878]

Mullineux S-T, Lafontaine DLJ. Mapping the cleavage sites on mammalian pre-rRNAs: where do we stand? Biochimie. 2012; 94:1521–1532. [PubMed: 22342225]

Neumuller RA, Gross T, Samsonova AA, Vinayagam A, Buckner M, Founk K, Hu Y, Sharifpoor S, Rosebrock AP, Andrews B, Winston F, Perrimon N. Conserved Regulators of Nucleolar Size Revealed by Global Phenotypic Analyses. Sci. Signaling. 2013; 6:ra70-ra70.

Neumüller RA, Betschinger J, Fischer A, Bushati N, Poernbacher I, Mechtler K, Cohen SM, Knoblich JA. Mei-P26 regulates microRNAs and cell growth in the Drosophila ovarian stem cell lineage. Nature. 2008; 454:241–245. [PubMed: 18528333]

Nicolas E, Parisot P, Pinto-Monteiro C, de Walque R, De Vleeschouwer C, Lafontaine DLJ. Involvement of human ribosomal proteins in nucleolar structure and p53-dependent nucleolar stress. Nat. Commun. 2016; 7:11390. [PubMed: 27265389]

Noguchi T, Miller KG. A role for actin dynamics in individualization during spermatogenesis in Drosophila melanogaster. Development. 2003; 130:1805–1816. [PubMed: 12642486]

Peculis BA. The sequence of the 5′ end of the U8 small nucleolar RNA is critical for 5.8S and 28S rRNA maturation. Mol. Cell. Biol. 1997; 17:3702–3713. [PubMed: 9199304]

Peculis BA, Steitz JA. Disruption of U8 nucleolar snRNA inhibits 5.8S and 28S rRNA processing in the Xenopus oocyte. Cell. 1993; 73:1233–1245. [PubMed: 8513505]

Pertschy B, Schneider C, Gnadig M, Schafer T, Tollervey D, Hurt E. RNA Helicase Prp43 and Its Co-factor Pfa1 Promote 20 to 18 S rRNA Processing Catalyzed by the Endonuclease Nob1. J. Biol. Chem. 2009; 284:35079–35091. [PubMed: 19801658]

Petfalski E, Dandekar T, Henry Y, Tollervey D. Processing of the precursors to small nucleolar RNAs and rRNAs requires common components. Mol. Cell. Biol. 1998; 18:1181–1189. [PubMed: 9488433]

Piper PW, Bellatin JA, Lockheart A. Altered maturation of sequences at the 3′ terminus of 5S gene transcripts in a Saccharomyces cerevisiae mutant that lacks a RNA processing endonuclease. EMBO J. 1983; 2:353–359. [PubMed: 11894949]

Piper PW, Patel N, Lockheart A. Processing of the 3′ sequence extensions upon the 5S rRNA of a mutant yeast in Xenopus laevis germinal vesicle extract. Eur. J. Biochem. 1984; 141:115–118. [PubMed: 6327301]

Preti M, O′Donohue M-F, Montel-Lehry N, Bortolin-Cavaillé M-L, Choesmel V, Gleizes P-E. Gradual processing of the ITS1 from the nucleolus to the cytoplasm during synthesis of the human 18S rRNA. Nucleic Acids Res. 2013; 41:4709–4723. [PubMed: 23482395]

Rassoulzadegan M, Grandjean V, Gounon P, Vincent S, Gillot I, Cuzin F. RNA-mediated non-mendelian inheritance of an epigenetic change in the mouse. Nature. 2006; 441:469–474. [PubMed: 16724059]

Roers A, Hiller B, Hornung V. Recognition of Endogenous Nucleic Acids by the Innate Immune System. Immunity. 2016; 44:739–754. [PubMed: 27096317]

Rorth P. Gal4 in the Drosophila female germline. Mech. Dev. 1998; 78:113–118. [PubMed: 9858703]

Sanchez CG, Teixeira FK, Czech B, Preall JB, Zamparini AL, Seifert JRK, Malone CD, Hannon GJ, Lehmann R. Regulation of Ribosome Biogenesis and Protein Synthesis Controls Germline Stem Cell Differentiation. Cell Stem Cell. 2016; 18:276–290. [PubMed: 26669894]

Schneider C, Kudla G, Wlotzka W, Tuck A, Tollervey D. Transcriptome-wide analysis of exosome targets. Mol. Cell. 2012; 48:422–433. [PubMed: 23000172]

Sharma S, Lafontaine DLJ. “View From A Bridge”: A New Perspective on Eukaryotic rRNA Base Modification. Trends Biochem. Sci. 2015; 40:560–575. [PubMed: 26410597]

Sheng XR, Posenau T, Gumulak-Smith JJ, Matunis E, Van Doren M, Wawersik M. Jak-STAT regulation of male germline stem cell establishment during Drosophila embryogenesis. Dev. Biol. 2009; 334:335–344. [PubMed: 19643104]

Silva S, Homolka D, Pillai RS. Characterization of the mammalian RNA Exonuclease 5/NEF-sp as a testis-specific nuclear 3”→5” exoribonuclease. RNA. 2017 rna.060723.117.

Sloan KE, Mattijssen S, Lebaron S, Tollervey D, Pruijn GJM, Watkins NJ. Both endonucleolytic and exonucleolytic cleavage mediate ITS1 removal during human ribosomal RNA processing. J. Cell Biol. 2013; 200:577–588. [PubMed: 23439679]

Smibert P, Bejarano F, Wang D, Garaulet DL, Yang J-S, Martin R, Bortolamiol-Becet D, Robine N, Hiesinger PR, Lai EC. A Drosophila genetic screen yields allelic series of core microRNA biogenesis factors and reveals post-developmental roles for microRNAs. RNA. 2011; 17:1997–2010. [PubMed: 21947201]

Srivastava L, Lapik YR, Wang M, Pestov DG. Mammalian DEAD box protein Ddx51 acts in 3′ end maturation of 28 S rRNA by promoting the release of U8 snoRNA. Mol. Cell. Biol. 2010; 30:2947–2956. [PubMed: 20404093]

Tadros W, Houston SA, Bashirullah A, Cooperstock RL, Semotok JL, Reed BH, Lipshitz HD. Regulation of maternal transcript destabilization during egg activation in Drosophila. Genetics. 2003; 164:989–1001. [PubMed: 12871909]

Tafforeau L, Zorbas C, Langhendries J-L, Mullineux S-T, Stamatopoulou V, Mullier R, Wacheul L, Lafontaine DLJ. The complexity of human ribosome biogenesis revealed by systematic nucleolar screening of Pre-rRNA processing factors. Mol. Cell. 2013; 51:539–551. [PubMed: 23973377]

Tautz D, Dover GA. Transcription of the tandem array of ribosomal DNA in Drosophila melanogaster does not terminate at any fixed point. EMBO J. 1986; 5:1267–1273. [PubMed: 16453684]

Tian Y, Simanshu DK, Ascano M, Diaz-Avalos R, Park AY, Juranek SA, Rice WJ, Yin Q, Robinson CV, Tuschl T, Patel DJ. Multimeric assembly and biochemical characterization of the Trax-translin endonuclease complex. Nat. Struct. Mol. Biol. 2011; 18:658–664. [PubMed: 21552261]

Udem SA, Warner JR. The cytoplasmic maturation of a ribosomal precursor ribonucleic acid in yeast. J. Biol. Chem. 1973; 248:1412–1416. [PubMed: 4568815]

van Hoof A, Lennertz P, Parker R. Three conserved members of the RNase D family have unique and overlapping functions in the processing of 5S, 5.8S, U4, U5, RNase MRP and RNase P RNAs in yeast. EMBO J. 2000; 19:1357–1365. [PubMed: 10716935]

Vesper O, Amitai S, Belitsky M, Byrgazov K, Kaberdina AC, Engelberg-Kulka H, Moll I. Selective translation of leaderless mRNAs by specialized ribosomes generated by MazF in Escherichia coli. Cell. 2011; 147:147–157. [PubMed: 21944167]

Watkins NJ, Bohnsack MT. The box C/D and H/ACA snoRNPs: key players in the modification, processing and the dynamic folding of ribosomal RNA. WIREs RNA. 2012; 3:397–414. [PubMed: 22065625]

Wei Y, Mizzen CA, Cook RG, Gorovsky MA, Allis CD. Phosphorylation of histone H3 at serine 10 is correlated with chromosome condensation during mitosis and meiosis in Tetrahymena. Proc. Natl. Acad. Sci. U. S. A. 1998; 95:7480–7484. [PubMed: 9636175]

Wickramasinghe VO, Venkitaraman AR. RNA Processing and Genome Stability: Cause and Consequence. Mol. Cell. 2016; 61:496–505. [PubMed: 26895423]

Wu H, Xu H, Miraglia LJ, Crooke ST. Human RNase III is a 160-kDa protein involved in preribosomal RNA processing. J. Biol. Chem. 2000; 275:36957–36965. [PubMed: 10948199]

Zemp I, Kutay U. Nuclear export and cytoplasmic maturation of ribosomal subunits. FEBS Lett. 2007; 581:2783–2793. [PubMed: 17509569]

Zhang Q, Shalaby NA, Buszczak M. Changes in rRNA transcription influence proliferation and cell fate within a stem cell lineage. Science. 2014; 343:298–301. [PubMed: 24436420]

Zhang X, Gao X, Coots RA, Conn CS, Liu B, Qian S-B. Translational control of the cytosolic stress response by mitochondrial ribosomal protein L18. Nat. Struct. Mol. Biol. 2015; 22:404–410. [PubMed: 25866880]

Zuo Y, Deutscher MP. Exoribonuclease superfamilies: structural analysis and phylogenetic distribution. Nucleic Acids Res. 2001; 29:1017–1026. [PubMed: 11222749]

Highlights

- Rexo5 exonuclease trims 3′ ends of snoRNAs, 28S and 5S rRNA precursor
- Loss of Rexo5 leads to nuclear retention of 18S ribosomal subunits
- Rexo5 is overexpressed in the germline and required for germline differentiation

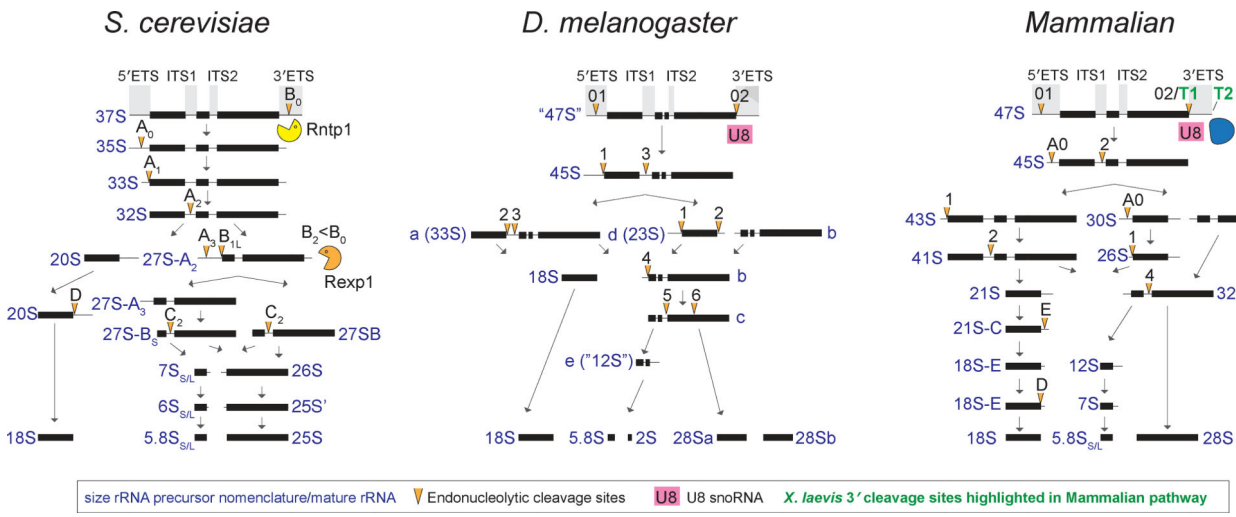

Figure 1. Overview of *S. cerevisiae, D. melanogaster* and mammalian rRNA biogenesis pathways

Sizes of rRNA intermediates are indicated in dark blue, endonucleolytic cleavage sites with orange arrows. S. cerevisiae: 37S pre-rRNA is cleaved in the 3′-ETS by Rnt1p dsRNA endonuclease (yellow). The 3′-5′ exonuclease Rex1p (orange) trims off the remaining trailer from 27S-A2 during late rRNA biogenesis (B0 to B2) (Mullineux and Lafontaine, 2012). D. melanogaster: rRNA biogenesis intermediates are generally conserved among verte- and invertebrates; 5.8S rRNA is cleaved into 2S and a short 5.8S and 28S rRNA fragments into 28Sa and 28Sb (Long and Dawid, 1980). U8 snoRNA is conserved (magenta) (Peculis, 1997). Mammalian: Cleavage site 02 is positioned at the 28S-3′-ETS border (Mullineux and Lafontaine, 2012). Release of 45S pre-rRNA depends on U8 snoRNA (magenta) (Peculis and Steitz, 1993). Murine Ddx51 helicase (blue) is required for U8 unwinding from 28S rRNA during 3′-ETS removal (Srivastava et al., 2010). X. laevis cleavage sites in the 3′-ETS T1 and T2 are shown in green.

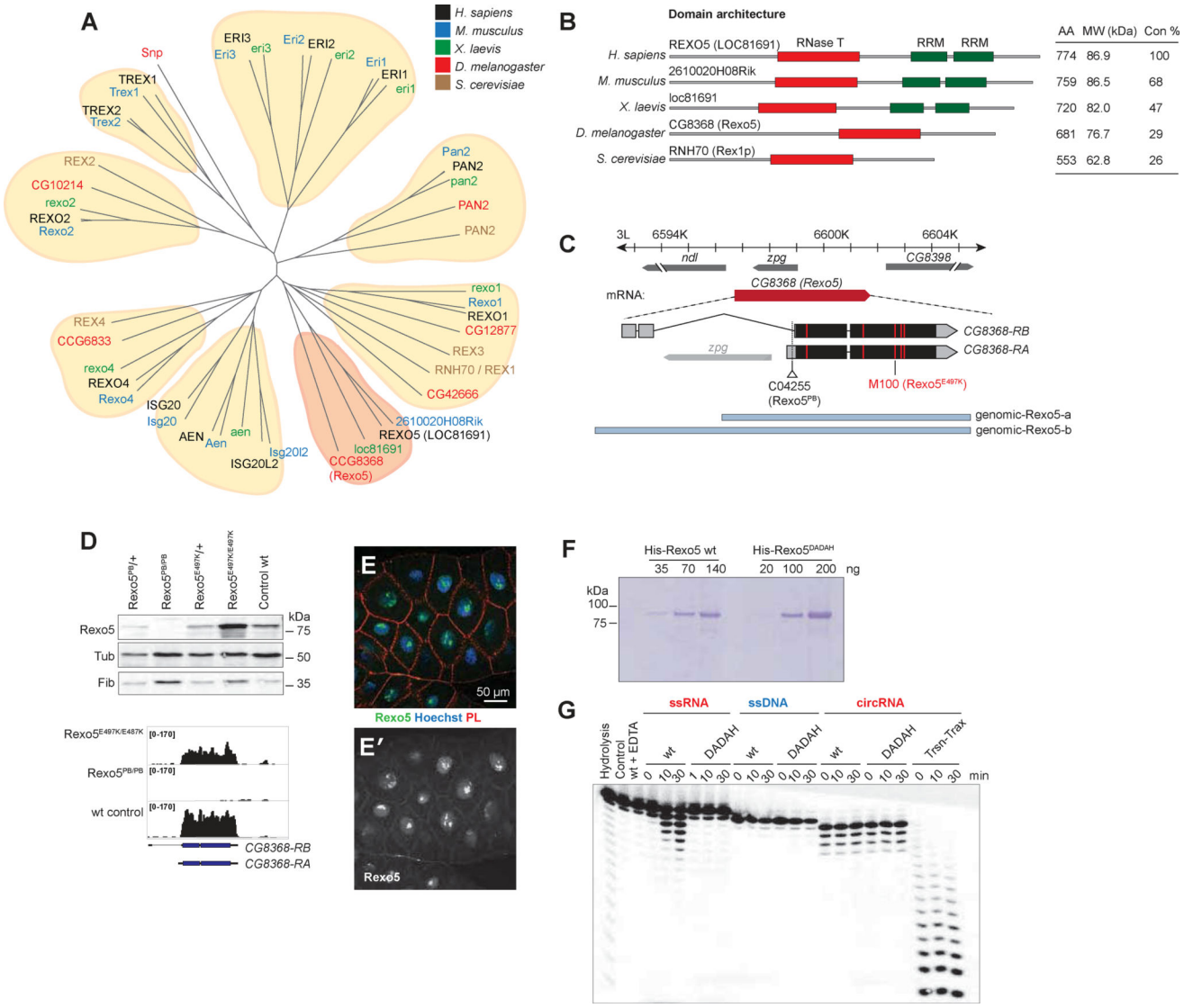

Figure 2. Rexo5 is a conserved RNA exonuclease essential for viability in *D. melanogaster*

(A) Phylogenetic tree of DEDDh RNase T 3′-5′ exonucleases in H. sapiens (black), M. musculus (blue), X. laevis (green), D. melanogaster (red), and S. cerevisiae (brown). Homologous families are grouped in yellow; Rexo5 orthologs are highlighted in orange. (B) Domain organization of Rexo5 exonucleases. S. cerevisiae RNH70/REX1/Rex1p groups with the paralogous REXO1 family. RNase T domains (red) and RRM domains (green) are drawn to scale relative to the total protein length. Amino acid length (AA), predicted molecular weight, and percentage conservation (Con%) to human REXO5 are shown in the table. (C) Rexo5 (CG8368) gene and mRNA isoforms. C04255 ($Rexo5^{PB}$) transposon insertion (triangle) and nucleotide substitutions within M1 00 ($Rexo5^{E497K}$) EMS point mutant (red lines) are indicated on the Rexo5 transcripts. Location of transgenic Rexo5 rescue constructs (light blue): genomic-Rexo5-a covers 1.6 kb of the promoter disrupting zpg, genomic-Rexo5-b covers 3.3 kb of the promoter and spans both Rexo5 isoforms. (D) Upper panel: Western blot analysis of endogenous Rexo5 in homo- and heterozygous mutants and wild-type L2 larvae. Alpha-Tubulin (Tub) and nucleolar Fibrillarin (Fib) are

loading controls. Lower Panel: mRNA-seq RPKM expression levels of Rexo5 in Rexo5 homozygous L2 mutants and wild-type controls. (E,E′) GFP-Rexo5 (green) localizes to nucleoli/nuclei in somatic cells: Salivary gland cells co-stained for actin (red, Phalloidin, PL) and DNA (blue, Hoechst). (F) Commassie gel of recombinant His-Rexo5 wild-type ($Rexo5^{wt}$) and mutant protein ($Rexo5^{DADAH}$) purified from baculoviral Sf9 cells. (G) In vitro RNA exonuclease assays of recombinant $Rexo5^{wt}$ and $Rexo5^{DADAH}$ protein visualized on a high resolution sequencing gel. RNase activity assays of $Rexo5^{wt}$ and $Rexo5^{DADAH}$ testing 5′-^{32}P-labeled poly(C) single strand RNA (ssRNA) and ssDNA 18-mer oligo(deoxy)ribonucleotides, and circularized poly(C) RNA (circRNA) at 20 nM enzyme and 100 nM RNA concentration in a time series (0–30 min). As controls, ssRNAs were incubated without enzyme (Control) or incubated with $Rexo5^{wt}$ and 50 mM EDTA for 30 min (wt + EDTA). The hydrolysis ladder (Hydrolysis): ssRNA incubated with a 50 mM KOH solution at 90°C for 5 min. The Translin-Trax complex was used an endonucleolytic enzyme control (Tian et al., 2011).

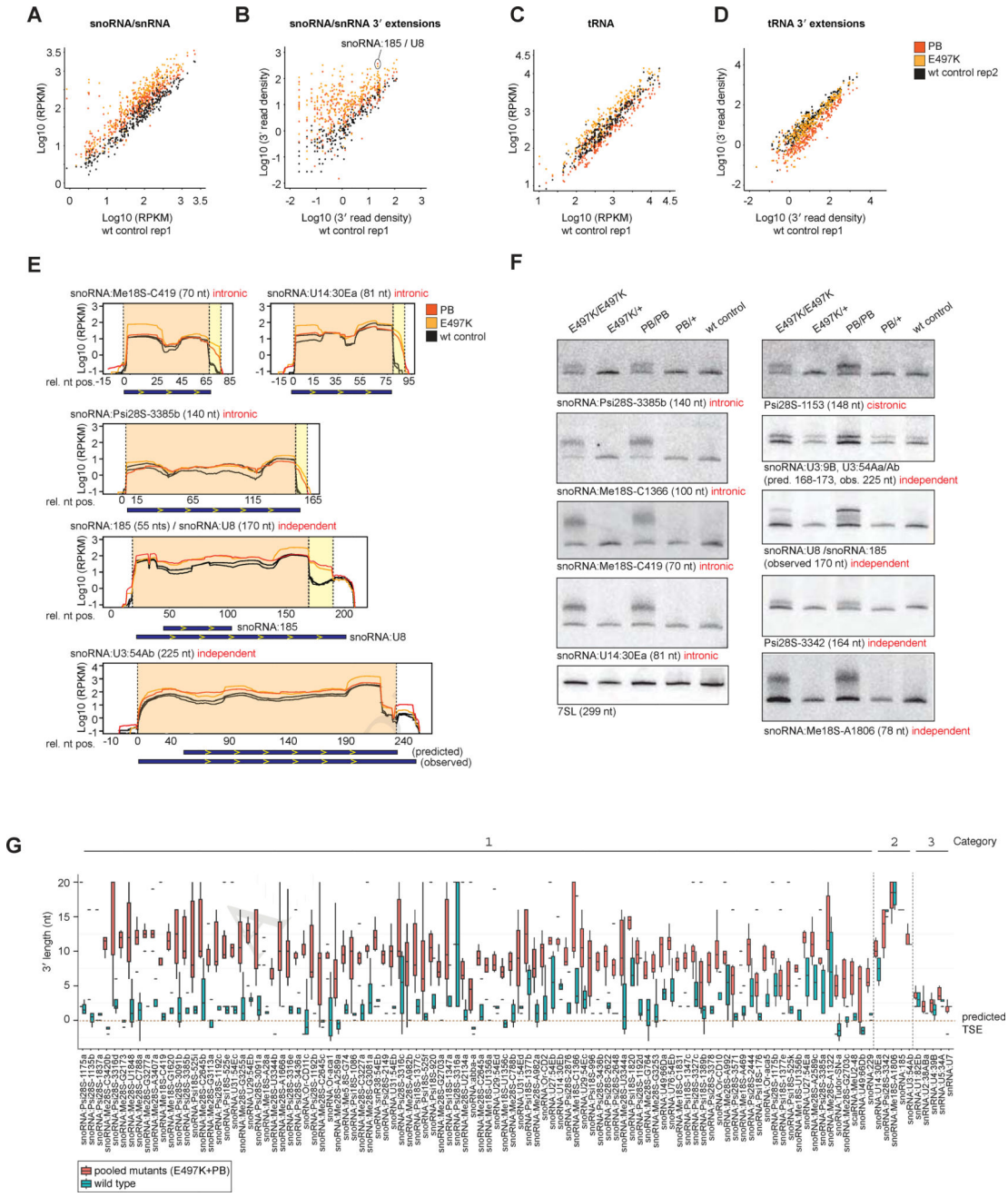

Figure 3. snoRNAs are globally extended at their 3′ ends in Rexo5 mutants

(A) Scatterplots of hydrolysis-based RNA-seq abundances (Log10 RPKM) of snRNAs and snoRNAs extended by 25 nt at the start and end coordinates. The x-axis shows RNA-seq abundances of wild-type L2 larvae (control wt rep1), the y-axis shows L2 homozygous mutants (E497K, Rexo5^{E497K}, orange; PB, Rexo5^{PB}, red) and wild-type L2 replicate 2 (control wt rep2, black). (B) Scatterplots of library-normalized read densities of 25-nt long windows at the 3′-termini of snoRNAs and snRNAs (3′ read density) for the same samples above. U8 snoRNA is marked (snoRNA:185/U8). (C,D) Same analysis as in (A,B) for tRNAs and tRNA 3′-termini. (E) Log10 RNA-seq coverage plots of selected snoRNAs for

homozygous Rexo5^{PB} (PB, red), Rexo5^{E497K} (E497K, orange), and control L2 larvae (wt control rep2, black). Official gene name, nucleotide length (black) and type of transcription locus (intronic, independent) (red) are shown above each coverage plot, the length of the mature snoRNA (blue bar) below. The location of the mature snoRNA is shaded in orange; the 3′ precursor region upregulated in mutants is highlighted in yellow. Nucleotide position is given relative to transcript start site. U8 snoRNA (170 nt) extends beyond the predicted snoRNA:185 (54 nt) gene locus. The observed read coverage for U3 snoRNA (225 nt) extends the predicted length (168–173 nt). (F) Northern blot analysis of selected snoRNAs for Rexo5^{PB} and Rexo5^{E497K} homo- and heterozygous mutants and wild-type L2 larvae. Official gene names, lengths (black), and type (intronic, cistronic, independent) (red) are indicated below each blot. The same blot was stripped and re-probed for all probes. Loading control is 7SL RNA. (G) 3′ length analysis of snoRNA and snRNA precursors recorded by hydrolysis-based small RNA-seq, averaging six homozygous L2 mutants (three Rexo5^{PB} and three Rexo5^{E497K} pooled together) (red) and four wild-type L2 larvae (green). The x-axis shows snoRNA and snRNA gene identifiers, the y-axis the average number of nucleotides (nt) extending beyond the annotated transcript end (3′ length). Category 1: Selection of snoRNAs with the largest precursor 3′-processing changes accumulating in mutants. Category 2: Subgroup of highly abundant snoRNAs, which accumulate misprocessed precursors in mutants by density reads analysis in (B), but also have precursor coverage of >2 reads in wild-type controls. Category 3: subset of snRNAs. snRNAs show no altered 3′ end by length analysis and read density analysis.

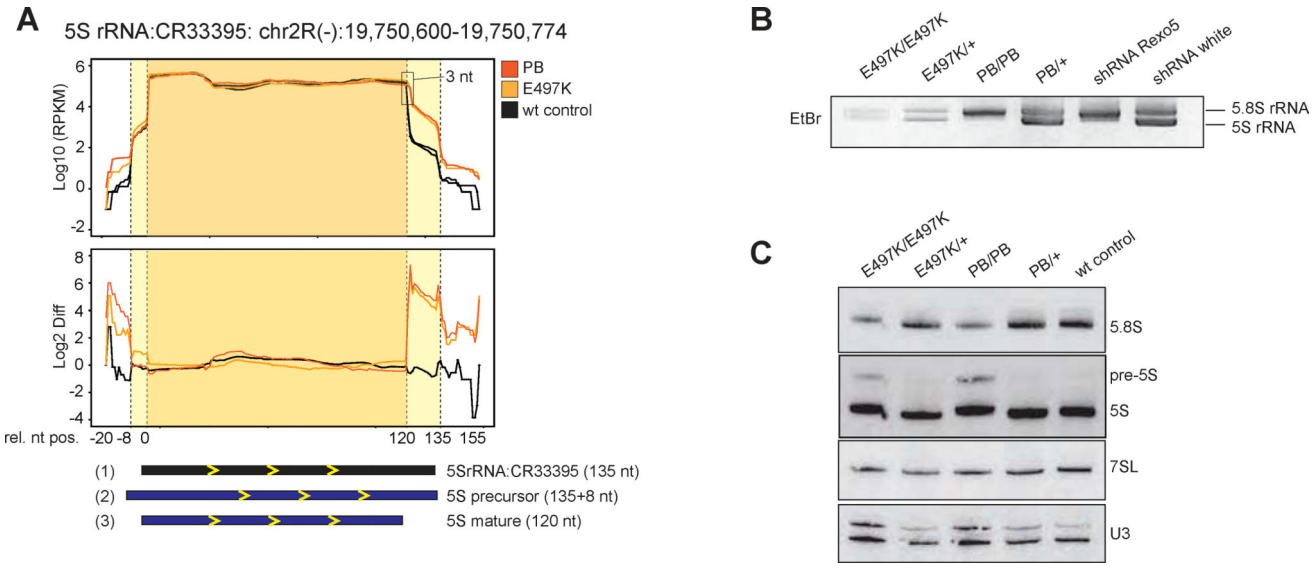

Figure 4. Rexo5 mutants accumulate 3′-extended 5S rRNA

(A) Upper panel: Log10 RPKM read coverage plots of 5S rRNA in L2 homozygous mutant larvae (PB, Rexo5^{PB}, red; E497K, Rexo5^{E497K}, orange) and wild-type controls (black, both replicates) sequenced by hydrolysis-based RNA-seq. Lower panel: Log2 fold changes of read coverages (Log2 Diff) between mutants and wild-type control rep1 (E497K orange; PB red) and wild-type rep1 versus wild-type rep2 (black). Shown below is (1) length of the Flybase annotated 5S rRNA gene CR33395 (blue bar), (2) length of the observed 5S rRNA precursor (black) and (3) observed mature 5S rRNA by RNA-seq coverage (black). Mature 5S rRNA is shaded in orange, the 3′ trailer of the precursor in yellow. (B) Ethidium bromide stained 8% polyacrylamide/8M urea gel showing a higher molecular weight shift for 5S rRNA in L2 homozygous mutants and Tubulin-GAL4 UAS-shRNA-Rexo5 knockdowns. (C) Northern blot analysis for 5S, 5.8S rRNAs, 7SL RNA and U3 snoRNA in hetero- and homozygous Rexo5 mutants and wild type controls.

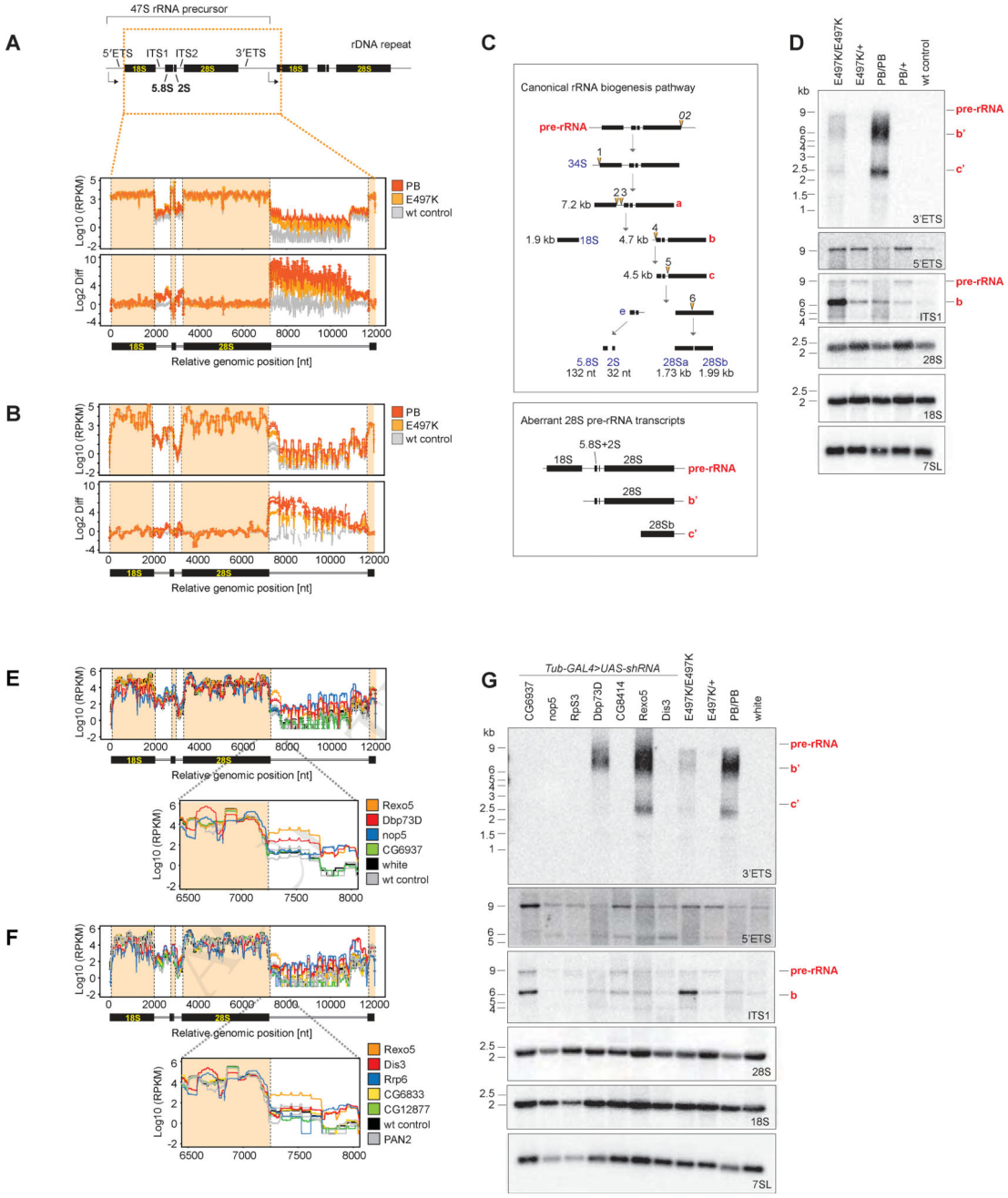

Figure 5. Rexo5 mutants accumulate 3′-ETS-containing 28S rRNA precursors

(A) Genomic map of rRNA precursors arranged in rDNA repeats. Location of the reference transcript M2017.1 used for alignments indicated with the dotted orange box. Upper panel: Hydrolysis-based RNA-seq read coverage (Log10 RPKM) of L2 homozygous mutants (PB, Rexo5^{PB} red; E497K, Rexo5^{E497K}, orange), and two replicate wild-type controls (gray). The location of mature 18S, 5.8S, 2S, and 28S rRNA is shown with the shaded orange areas. Lower panel: Log2-transformed coverage changes (Log2 Diff) between mutants and one wild-type control (same color code as in (A)) and coverage changes between two wild-type replicates (gray). (B) Same as in (A) for Illumina total RNA-seq (>200 nt read selection).

(C) Canonical rRNA biogenesis pathway in D. melanogaster (Long and Dawid, 1980); cleavages sites are indicated with orange arrows. 28S rRNA hydrolytically fragments into 28Sa and 28Sb, which electrophoretically migrate close to 18S rRNA (Jordan, 1975). rRNA intermediates misprocessed in mutants are highlighted in bold red. (D) Northern blot analysis of rRNA precursors in homo- and heterozygous Rexo5^{E497K} (E497K/E497K; E497K/+) and Rexo5^{PB} (PB/PB; PB/+) and L2 wild-type larvae, probed for 5′-ETS, ITS1, mature 18S, mature 28Sb, 3′-ETS, and 7SL RNA as loading control. (E) Log10 RPKM read coverage plots along M2017.1 for in vivo Tubulin-GAL4 UAS-shRNA knockdowns (human ortholog in parentheses): Dbp73D (DDX51, red), nop5 (NOP58, blue), CG6937 (NIFK, green) and Rexo5 (LOC81691, orange), control shRNA knockdown of white (black), and wild-type L2 larvae (gray). Except for PAN2 and white, all knockdowns were lethal at L1 or L2. The 28S-3′-ETS transition is magnified in the box below. (F) Same as in (E) for 3′-5′ RNA exonucleases: Rexo5 (orange), Dis3 (red), Rrp6 (EXOSC10, blue), CG6833 (REXO4, yellow), genetic mutant CG12877^{e00300} (REXO1, green), PAN2 (gray), compared to control white (black). (G) Northern blot analysis probing for 3′-ETS, 5′-ETS, ITS1, 28S, 18S, and 7SL of shRNA knockdowns of nop5, RpS3, CG6937, Rexo5 and Dpb73D. All blots were stripped and re-probed for all probes.

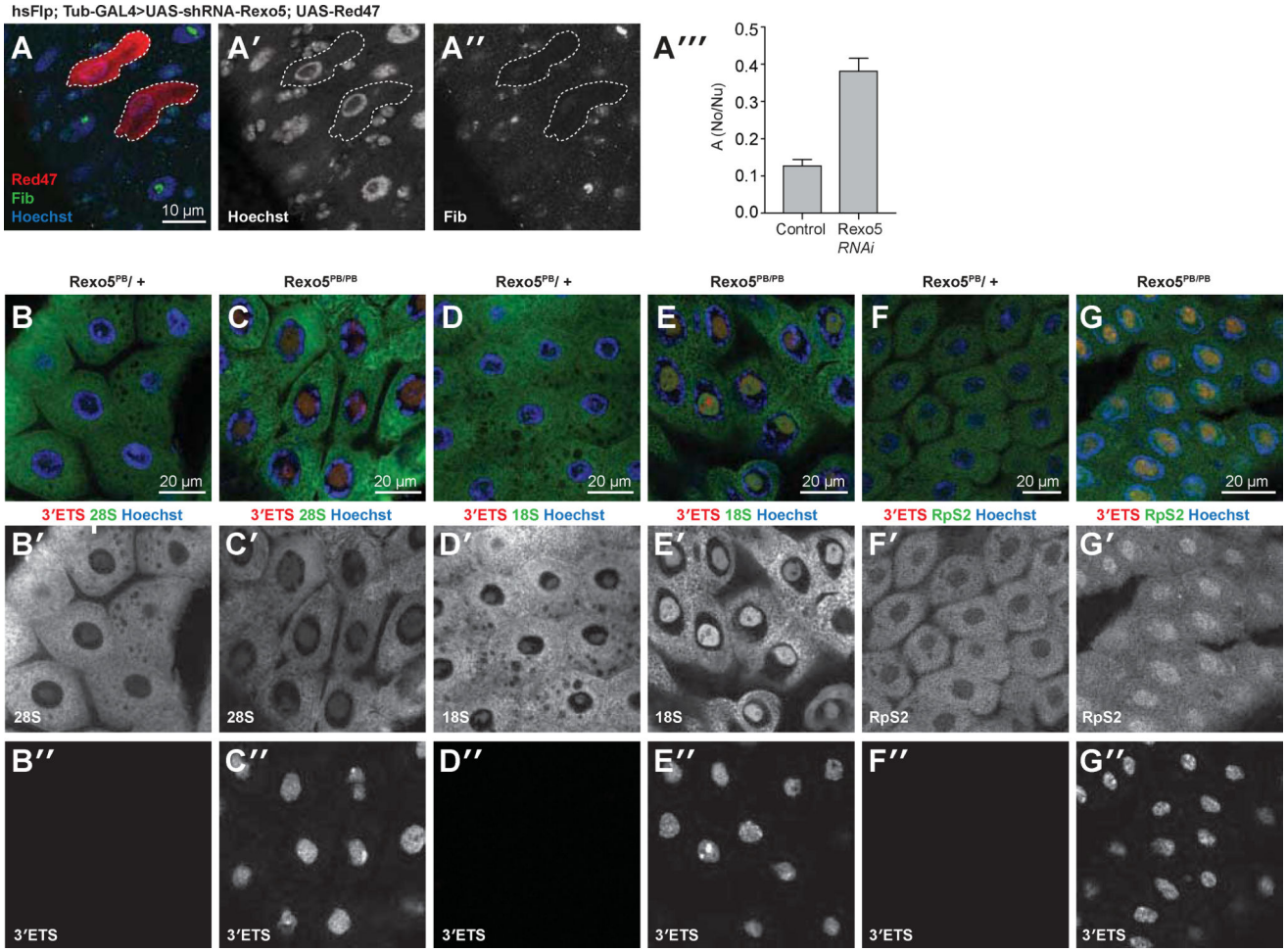

Figure 6. Rexo5 homozygous mutants display increased nucleolar size and show nuclear accumulation of RpS2

(A) Confocal image of Rexo5 RNAi clones in the midgut of L3 larvae. Cells expressing UAS-shRNA Rexo5 express UAS-Red47 (red). The nucleolar protein Fibrillarin (Fib) is stained in green, DNA (Hoechst) in blue. RNAi UAS-Red47 cells are circled with a white dashed line. Genotype: hsFlp; Tubulin-GAL4/UAS-shRNA-Rexo5; hsFlp;Sco/Cyo;UAS#Red47a#1tub<+GFP<GAL4/TM6B. Gray scale image of (A′) Hoechst and (A″) Fibrillarin staining. (A‴) Quantification of nuclear/nucleolar area ratios in shRNA knockdown (n=4) and wild-type cells (n=6), based on Hoechst stainings, which leaves the nucleolar area unstained. (B–C) RNA-FISH probing against the 3′-ETS (red) and mature 28S rRNA (green) in (B-B″) heterozygous ($Rexo5^{PB}$/+) and (C-C″) homozygous ($Rexo5^{PB/PB}$) L2 larvae. (B′, C) Gray scale images of 28S rRNA and (B″, C″) the 3′-ETS. (D–E) RNA-FISH probing against the 3′-ETS (red) and mature 18S rRNA (green) in (D-D″) heterozygous ($Rexo5^{PB}$/+) and (E-E″) homozygous ($Rexo5^{PB/PB}$) L2 larvae. (D′,E′) Gray scale images of 18S rRNA and (D″,E″) the 3′-ETS. (F–G) RNA-FISH probing against the 3′-ETS (red) in an RpS2-GFP (green) $Rexo5^{PB}$ genetic background. (F-F″) *In vivo* localization of RpS2-GFP (green) and the 3′-ETS (red) in (F) heterozygous ($Rexo5^{PB}$/+) and (G) homozygous ($Rexo5^{PB/PB}$) L2 mutant larvae. Nuclei are marked with Hoechst (blue). (F,G′) Gray scale images for RpS2-GFP and (F″,G″) the 3′-ETS.

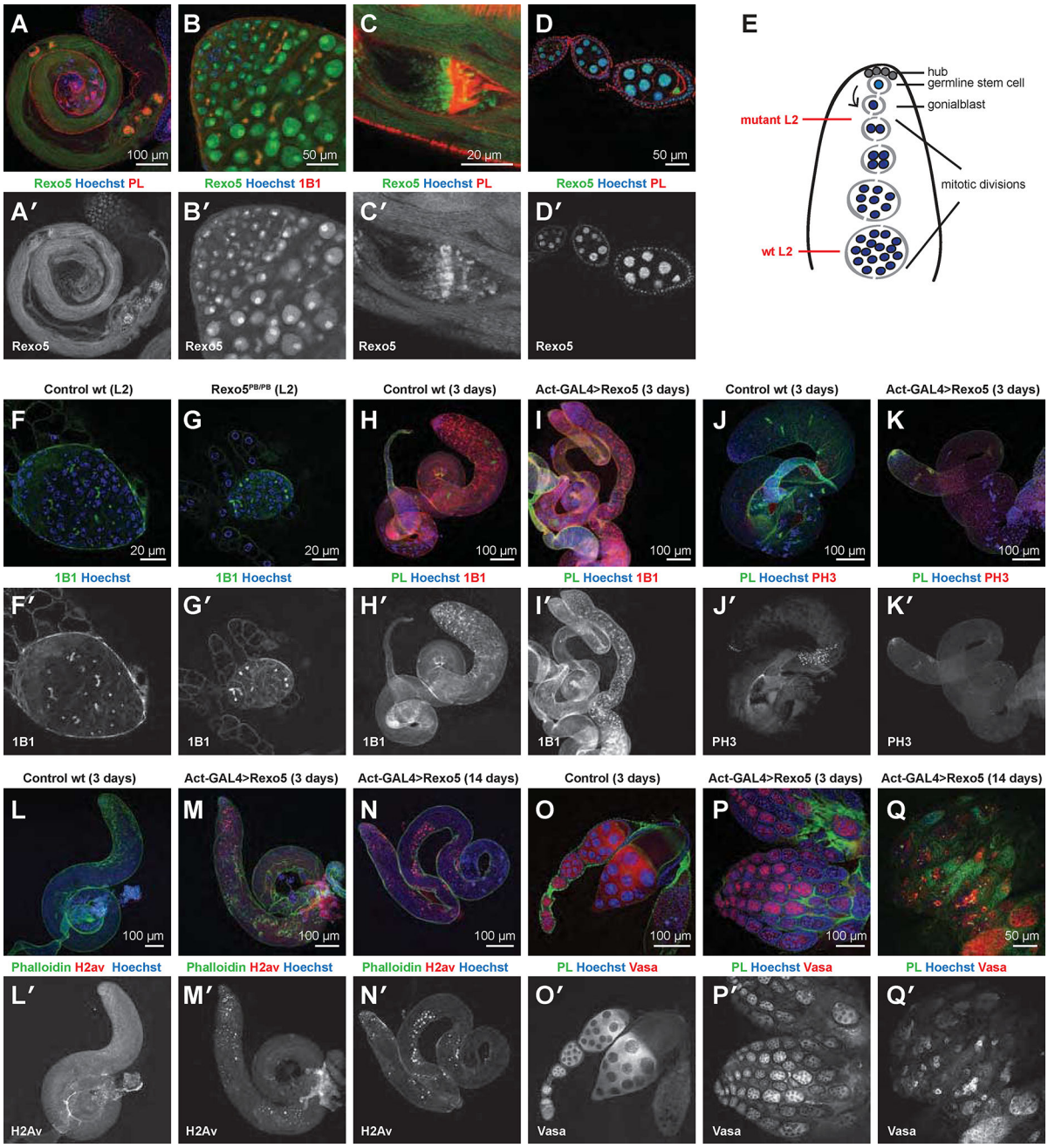

Figure 7. Loss-of-function of Rexo5 causes mitotic and growth arrest in male and female gonads

(A–D) Confocal imaging of transgenic GFP-Rexo5 under its native promoter; GFP-Rexo5 in green, DNA in blue (Hoechst), Phalloidin (A,C,D) or intracellular fusome marker 1B1 (B) are shown in red. (A–C) GFP-Rexo5 expression in adult testes (A,A′), at the testis apical tip (B,B′), in the cystic bulge (C,C). (D,D′) Rexo5 expression in adult ovarioles. (E) Schematic representation of the mitotic developmental program of *Drosophila* testis. Germ stem cells asymmetrically divide to produce one daughter stem cell and one gonialblast cell. The gonialblast migrates from the hub and undergoes four mitotic divisions. Stages of mutant and wild-type gonadal development at L2 are highlighted in red. (F,F) L2 wild-type male

gonads stained for 1B1 (green) and DNA (blue). (F) 1B1 gray scale image. (G,G) Same staining as in (F,F′) for L2 Rexo5^{PB} homozygous mutants. (H–M) Rexo5 mutants are lethal, but transgenic expression of pUASt-Rexo5 with Actin-GAL4 rescues somatic lethality to give adult flies that lack Rexo5 expression in germ cells (Brand and Perrimon, 1993). (H–I) 3-day-old adult wild-type and mutant testes. (H,H) Wild-type testes stained for actin (green, Phalloidin, PL), DNA (blue), and 1B1 (red). Mitotic cells (1B1) are restricted to the apical tip of the testis. (H) 1B1 gray scale image, (I,I′) Same as in (H,H) for Rexo5$^{PB/E497K}$ mutant testes. Mitotic cells are present throughout the entire testicular tube. (J,J′) 3-day old adult wild-type testis stained for Serine 10 phosphorylated histone H3 (PH3, red) marking meiotic nuclei. (J′) PH3 gray scale image. (K,K′) PH3 staining in mutant testes shows absence of meiotic nuclei. (L,L′) 3-day-old wild-type adult testis stained for phospho-H2av (red), Phalloidin (green), DNA (blue), (L′) gray scale image for H2Av. (M,M′) same as in (L,L′) for 3-day-old Actin-GAL4>Rexo5 Rexo5$^{PB/E497K}$ mutant testes. (N,N′) same as in (L,L′) for 14-day-old Actin-GAL4>Rexo5 rescued Rexo5^{E497K}/Df(3L)BSC411 mutant testes. (O,O′) Wild-type ovarioles at 3 days, Actin-GAL4 UAS-Rexo5 Rexo5^{PBE497K} mutant ovaries at 3 days (P,P′) and 14 days (Q,Q′), stained for Vasa (red), Phalloidin (green), DNA (blue).